

# Post shut-in hazard for hydraulic-fracturing-induced earthquakes: Analysis using data from the Guy-Greenbrier earthquake sequence

Ganyu Teng

Jack W. Baker

## Abstract

This project evaluates the existing statistical models to describe post-shut-in seismicity for hydraulic-fracturing-induced earthquakes and studies the importance of post-shut-in seismicity on decision-making. We focus on the short-term hazard based on the seismicity during and after the injection. We consider the Omori model by Langenbruch and Shapiro (2010), the exponential model, and the stretched exponential model from Mignan et al. (2017). In particular, we evaluate their performance on nine earthquake clusters that occurred in 2010 near the Guy-Greenbrier fault in Arkansas (using data from Yoon et al., 2017). While many of the post-shut-in sequences could be described by a single decay process, there is an increase in the post-shut-in seismicity in some clusters. Results show that the Omori model performs the best for the former case, while the stretched exponential model could capture the latter situations. We then use the Omori model to explore the effect of shut-in timing on the short-term hazard. Results show that the post-shut-in seismicity could affect the decision significantly for a slower decay in seismicity and longer injection duration. We perform a sensitivity analysis considering the uncertainties in the Omori model and the Gutenberg-Richter distribution. Results show that their relative importance depends on the injection duration and intensity thresholds of interest. Finally, we propose a logic tree model to incorporate the uncertainty in model selection and parameter estimation. The logic tree assembles the Omori model and the stretched exponential model to consider the possibility of increasing post-shut-in seismic hazard. We also show that each branch’s weight could be updated in a Bayesian manner with new data.

## 1 Introduction

Past studies of hydraulic-fracturing-induced earthquakes have observed that the seismicity does not always stop instantly after injection ceases (Langenbruch and Shapiro, 2010; Kao et al., 2018; Kim, 2013; Häring et al., 2008; Yoon et al., 2017). Some studies have observed that the frequency of seismic events can even increase after the shut-in (Majer et al., 2007; Deichmann and Giardini, 2009). As a result, it is important to consider and quantify the post-shut-in seismic hazard during decision-making.

There have been various statistical (e.g., Langenbruch and Shapiro, 2010; Broccardo et al., 2017; Mignan et al., 2017; Bachmann et al., 2011; Mena et al., 2013) and physics-based models (e.g., Chang et al., 2018; Segall and Lu, 2015; Gischig and Wiemer, 2013) developed to quantify the continuing seismicity after the termination of the injection. Langenbruch and Shapiro (2010) modified Omori’s Law to describe the decay in the seismicity after the shut-in. Mignan et al. (2017) and Broccardo et al. (2017) used exponential functions to describe post-shut-in seismicity. Mignan et al. (2017) developed a traffic light system considering both pre-shut-in and post-shut-in seismicity. Broccardo et al. (2017) also used Bayesian inference and updating rules to develop a probabilistic model that forecasts the induced seismicity. Bachmann et al. (2011) found that the aftershock sequence model (i.e., OmoriUtsu law) can provide an acceptable fit to the post-shut-in

seismicity for geothermal reservoir enhancement. They also modified the Epidemic Type Aftershock Sequence (ETAS) model to account for the flow rate in the seismic forecast. Mena et al. (2013) introduced a method by combining models from Reasenberg and Jones (1989), Hainzl and Ogata (2005) and Shapiro et al. (2010) to forecast the hazard for geothermal reservoir enhancement in Basel, Switzerland.

Physics-based models have also been developed based on the underlying physical process. Chang et al. (2018) and Dieterich et al. (2015) developed models to simulate the stress change after the shut-in and used them to predict the post-shut-in seismicity. Segall and Lu (2015) considered poroelastic and earthquake nucleation effects in the simulation and observed that a sudden shut-in could increase the seismicity locally. Gischig and Wiemer (2013) modeled seismicity based on the pressure diffusion and irreversible permeability enhancement.

Most of the above case studies are for geothermal reservoir enhancement in Europe, and there have been limited studies on the post-shut-in seismicity for hydraulic-fracturing-induced earthquakes in the U.S. Moreover, limited research has been done to quantify the impact of the post-shut-in hazard on decision-making. As a result, this study aims to evaluate the existing statistical models for post-shut-in seismicity for hydraulic-fracturing-induced earthquakes and explore its impact on decision-making during the operation. We also develop a logic tree model combining different statistical models to have a more robust and conservative hazard forecast.

To study the importance of post-shut-in seismicity on decision-making, we compute the short-term hazard based on seismicity during and after the injection. In particular, we define the short-term hazard as the expected number of times exceeding a modified Mercalli intensity ( $MMI \geq x$ ) at the injection site over the next  $T_E$  days given the current injection duration of  $T_S$  days. Figure 1 visualizes the scenario. The green shaded area between  $T_S$  and  $T_S + T_E$  contributes to the short-term hazard.  $T_{SI}$  is the actual shut-in time. We compare the hazard levels between cases with and without post-shut-in seismicity (i.e., the area highlighted in red in Figure 1) and explore the change in the decision on the shut-in timing.

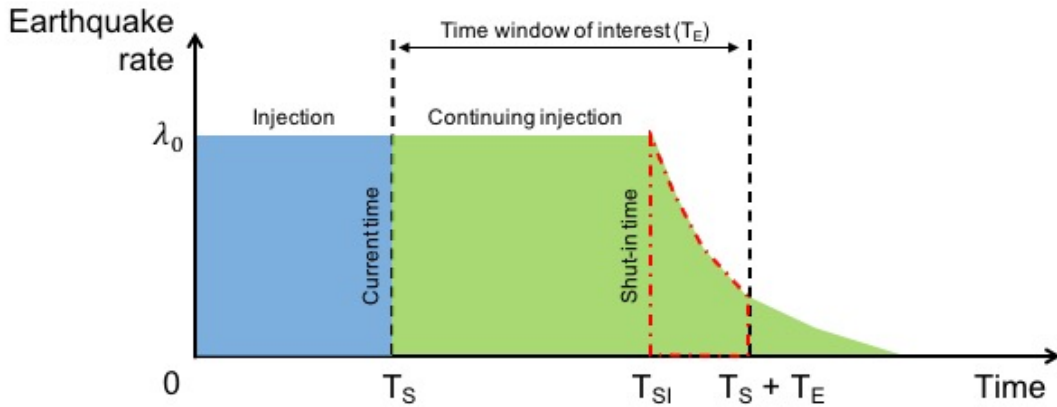


Figure 1: The setup for hazard analysis.  $T_S$  is the current injection time and  $T_{SI}$  is the shut-in time to be decided.  $T_E$  is the time range of interest. The area highlighted by the red line corresponds to the post-shut-in seismicity that contributes to the hazard. We assume a constant seismic rate during the injection (i.e.,  $\lambda_0$ ).

## 2 Data and processing

We consider earthquake and injection data from Yoon et al. (2017), who detected 14,604 earthquakes with  $-1.5 \leq M_L \leq 2.9$  near the Guy-Greenbrier fault in Arkansas from July 2010 to September 2010 (referred to hereafter as the ‘Guy-Greenbrier sequence’). The magnitude of completeness ( $M_c$ ) is 0.1 according to the Goodness of Fit test at the 95% level (Wiemer and Wyss, 2000). Yoon et al. (2017) detected and located microearthquakes in the Guy-Greenbrier sequence with two waveform similarity-based event detection methods. They grouped the earthquakes into 16 clusters and interpreted each as either hydraulic-fracturing-induced, wastewater-injection-induced, or natural seismicity. Moreover, Yoon et al. (2017) also associated each cluster with nearby injection wells.

To study the post-shut-in hazard for hydraulic-fracturing-induced earthquakes, we considered nine clusters that were well associated with hydraulic fracturing and had recorded post-shut-in seismicity. Of the omitted clusters, six were not associated with hydraulic fracturing, and one had has associated with hydraulic fracturing but had no post-injection seismicity. We collected all earthquakes with magnitudes above 0.2. Figure 2 summarizes the earthquake occurrence of the nine clusters, where the x-axis represents the time normalized by the shut-in time ( $T_{SI}$ ), and the y-axis is the cumulative number of earthquakes normalized by the number of earthquakes induced during the injection. Some of the clusters (i.e., Clusters 7 and 9) have many more post-shut-in earthquakes than pre-shut-in earthquakes, while for others (i.e., Clusters 1, 2, and 4), most of the earthquakes occur during the injection. Detailed earthquake sequences and injection information are included in the appendix. For many clusters, the earthquake occurrence rates drop after shut-in, while for other clusters, there is a surge in the seismicity after the shut-in.

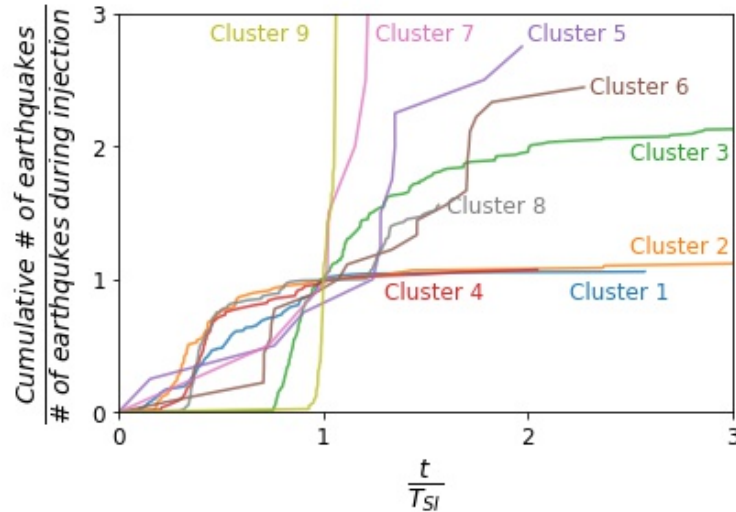


Figure 2: Earthquake occurrence for the nine clusters. The x-axis is the time normalized by the shut-in time ( $T_{SI}$ ), and y-axis is the cumulative number of earthquakes normalized by the earthquakes induced during the injection.

We considered three statistical models introduced in Langenbruch and Shapiro (2010) and Mignan et al. (2017). We did not consider physics-based models or more complex statistical models such as the ETAS model because of the limited earthquake data available and the complexity involved in calibrating the models for these situations. Langenbruch and Shapiro (2010) modified

Omori’s Law to describe the decay of seismicity after the shut-in (hereafter the Omori model):

$$\lambda(t) = \lambda_0 \left( \frac{T_{SI}}{t} \right)^p \quad (1)$$

where  $\lambda(t)$  is the seismicity rate at time  $t$ ,  $\lambda_0$  is the initial seismic rate,  $p$  describes the decay rate,  $T_{SI}$  is the duration of fluid injection, and  $t \geq T_{SI}$  is the time of interest. All the times are measured with respect to the start of the injection. Mignan et al. (2017) used exponential functions to describe the decay in seismicity after the shut-in (hereafter the exponential model):

$$\lambda(t) = \lambda_0 \exp \left( -\frac{t - T_{SI}}{\tau} \right) \quad (2)$$

where  $\tau$  is the parameter describing the decay in seismic rate after shut-in.

Both of the above models describe the post-shut-in seismicity as a single decay sequence, with the rate capped at  $\lambda_0$ . However, some past observations indicate that the seismicity is higher after shut-in (Segall and Lu, 2015; Majer et al., 2007; Deichmann and Giardini, 2009). Mignan et al. (2017) also described a stretched exponential model that could handle situations where post-shut-in seismicity is higher than  $\lambda_0$  (hereafter the stretched exponential model):

$$\lambda(t) = \lambda_0 (t - T_{SI})^{\beta-1} \exp \left( - \left( \frac{t - T_{SI}}{\tau} \right)^\beta \right) \quad (3)$$

where  $\tau$  and  $\beta$  are the parameters to be estimated.

### 3 Model evaluation

We evaluated the performances of the three models on the nine clusters in the Guy-Greenbrier sequence. For every cluster, we fitted the model using maximum likelihood estimation. In particular, for a non-homogeneous Poisson process with rate  $\lambda(t)$ , the likelihood can be computed using (Utsu et al., 1995):

$$L = \left\{ \prod_{i=1}^N \lambda(t_i) \right\} \exp \left\{ - \int_{T_s}^{T_e} \lambda(t) dt \right\} \quad (4)$$

where  $N$  is the number of post-shut-in earthquakes in each cluster, and  $t_i$  is the occurrence time of  $i^{th}$  earthquake with respect to the injection start time. For cases with overlapped injections, we considered the start of the earliest injection as the injection start time and the end of the last injection as the shut-in time.  $\lambda(t_i)$  is the seismicity rate at time  $t_i$  using one of the three models. We estimated the daily rate at the shut-in time ( $\lambda_0$ ) as the number of earthquakes the day before the shut-in (i.e.,  $T_{SI} - 1 \leq t_i \leq T_{SI}$ ). This worked well for the considered clusters, but other time-windows for rate estimation could be considered. If the estimated  $\lambda_0$  is zero, we set it to a small constant (i.e., 0.01) for ease of computation.  $T_s$  and  $T_e$  define the time window of the post-shut-in seismicity. We set  $T_s$  as the injection shut-in time (i.e.,  $T_s = T_{SI}$ ). For the interest of short-term hazard analysis, we set  $T_e$  as 30 days after shut-in, or the start of the next injection activity, or the end of the catalog according to Yoon et al. (2017), whichever is earlier. This time window included the majority of post-shut-in earthquakes for the clusters considered.

After fitting the cluster using maximum likelihood estimation, we evaluated the performance of the three models based on their Bayesian information criterion (BIC):

$$BIC = k \log(N) - 2 \log(\hat{L}) \quad (5)$$

where  $k$  is the number of parameters estimated by the model,  $\hat{L}$  is the estimated likelihood for every cluster, and  $N$  is the number of post-shut-in earthquakes. BIC is a popular model selection metric that balances the data fit to a model with the number of model parameters. A model with a lower BIC value is preferred (Schwarz, 1978).

Table 1 and Figure 3 summarize the BIC values normalized by the number of post-shut-in earthquakes (so that comparisons across clusters with differing numbers of earthquakes are easier). Figures 4 to 7 show the fitted rates for a few selected clusters. The fitted models for all clusters are included in the appendix. Results show that the Omori model or the stretched exponential model has the lowest BIC. In particular, for clusters where the seismicity decays monotonically after the shut-in (i.e., Clusters 1 to 4), the Omori model outperforms the other two. For clusters with an increase in post-shut-in seismicity (e.g., Clusters 7 to 9), the stretched exponential model performs the best.

Table 1: BIC values computed from Equation 5 normalized by the number of post-shut-in earthquakes, for the nine considered clusters. Black text indicates the most efficient model for the given cluster.

Cluster index	Omori	Exponential	Stretched exponential
<b>1</b>	0.42	1.56	0.42
<b>2</b>	2.96	3.42	3.38
<b>3</b>	-3.10	-2.09	-2.69
<b>4</b>	3.26	3.44	3.73
<b>5</b>	1.44	1.0	0.98
<b>6</b>	2.21	2.03	1.0
<b>7</b>	9.25	9.25	0.26
<b>8</b>	-1.73	-1.73	-3.58
<b>9</b>	-5.19	-5.31	-5.40

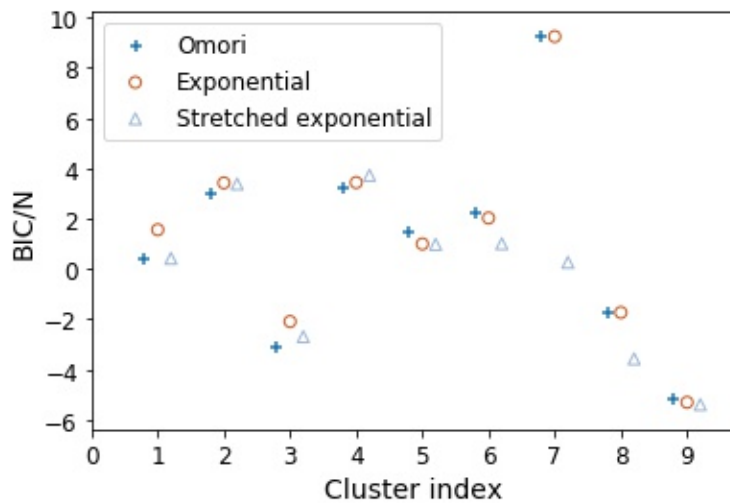


Figure 3: BIC of every cluster normalized by their corresponding number of post-shut-in earthquakes. Results for a given cluster are slightly offset horizontally, to avoid overlap.

Both the Omori and the exponential models are single decay models (i.e., the seismicity decays monotonically). Compared to the stretched exponential model, the single decay model parameter is easier to estimate and interpret. They work well when the seismicity decays monotonically after the shut-in, which is valid for many clusters (e.g., Clusters 1 to 4). However, the seismic rate for a single decay model is capped at  $\lambda_0$ . Thus it fails to capture the case when there are delayed earthquake clusters after shut-in or when the seismicity increases after shut-in. As a result, a single decay model could underestimate the post-shut-in hazard. This situation could be better described by the stretched exponential model, especially if there is a delayed earthquake cluster after shut-in (e.g., Cluster 8 in Figure 7). The time delay between the stimulation and the rapid increase in seismicity has been observed for hydraulic-fracturing-induced earthquakes (Yoon et al., 2017; Schultz et al., 2015), possibly due to the propagation time of the fluid pressure. As shown in Table 1, the stretched exponential model performs best for clusters with post-shut-in seismicity higher than  $\lambda_0$  (i.e., Clusters 5 to 9). Moreover, it also works for the single decay process (Figures 4 and 5). However, compared to single decay models, it is hard to interpret the two parameters of the stretched exponential model, especially for a limited number of clusters available. We noticed that large values of  $\beta$  and  $\tau$  lead to unphysical extrapolations to extreme seismicity rates. Thus, with limited clusters available, we set  $\beta$  and  $\tau$  below 20 during estimations. The stretched exponential model (like the other two models) also does not work well for more complex patterns, such as Cluster 7 in Figure 6 where there are multiple earthquake clusters after the shut-in. This could be improved by using a more complex model such as the ETAS model. Moreover, the stretched exponential model often results in a discontinuous rate right after shut-in. For example, Figure 5 shows a dramatic increase in the seismicity right after shut-in.

Since the single decay model is robust for parameter estimation and model interpretation, we utilize the Omori model below for demonstrations of hazard analysis calculations.

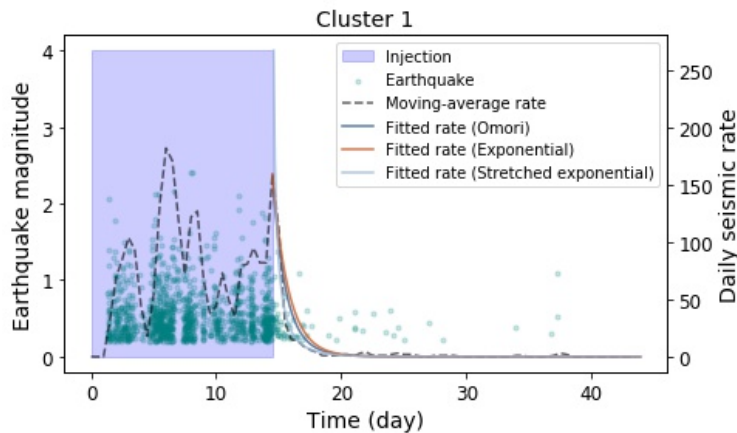


Figure 4: Earthquake occurrence of Cluster 1. The dots are earthquakes, with heights indicating their magnitudes. The shaded area corresponds to the injection. The dashed line is the recorded seismic rate, and the solid lines are the seismic rates using the three fitted models.

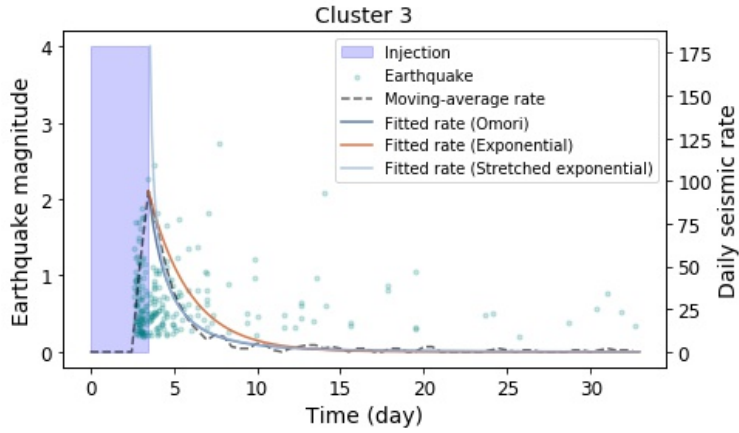


Figure 5: Earthquake occurrence of Cluster 3. The dots are earthquakes, with heights indicating their magnitudes. The shaded area corresponds to the injection. The dashed line is the recorded seismic rate, and the solid lines are the seismic rates using the three fitted models.

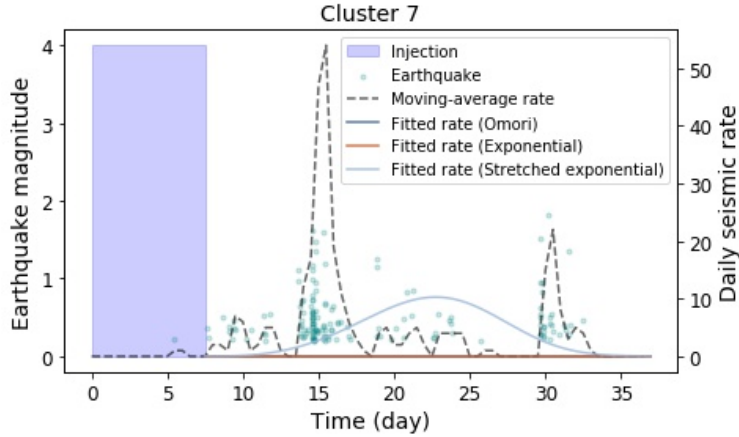


Figure 6: Earthquake occurrence of Cluster 7. The dots are earthquakes, with heights indicating their magnitudes. The shaded area corresponds to the injection. The dashed line is the recorded seismic rate, and the solid lines are the seismic rates using the three fitted models.

## 4 Post-shut-in hazard analysis and sensitivity study

### 4.1 The Omori model

We first studied the effect of the Omori model parameter  $p$  across all clusters. Figure 8 summarizes the  $p$  value for every cluster, with a median value of 2.2. This is consistent with Langenbruch and Shapiro (2010) where  $p$  of 2.0 is used as a reference value. Cluster 1 has a much higher  $p$ , indicating a dramatic decay in the post-shut-in seismicity. We then explored the relationship between the pre-shut-in information (e.g., injection volume, injection duration, and the number of earthquakes during the injection) and the  $p$  values. We conducted a linear regression between pairs of those pre-shut-in variables and  $p$ . Though Barth et al. (2013) suggested that  $p$  would be higher if the reactivated fracture system is in a stable state of stress (i.e., a large increase in pore pressure is required for fracture failure), we did not observe a statistically significant relationship between any pair. This is probably because of the limited data available and because not all clusters could

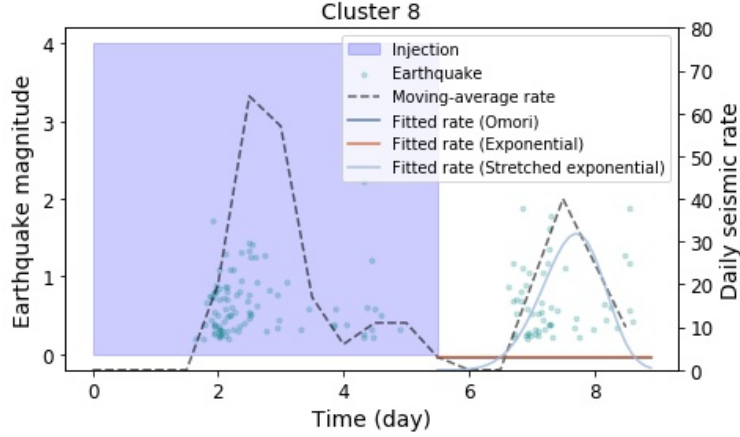


Figure 7: Earthquake occurrence of Cluster 8. The dots are earthquakes, with heights indicating their magnitudes. The shaded area corresponds to the injection. The dashed line is the recorded seismic rate, and the solid lines are the seismic rates using the three fitted models.

be well described as a single decay process. For illustration purposes, we assumed  $p = 2$  for the hazard analysis in the following section.

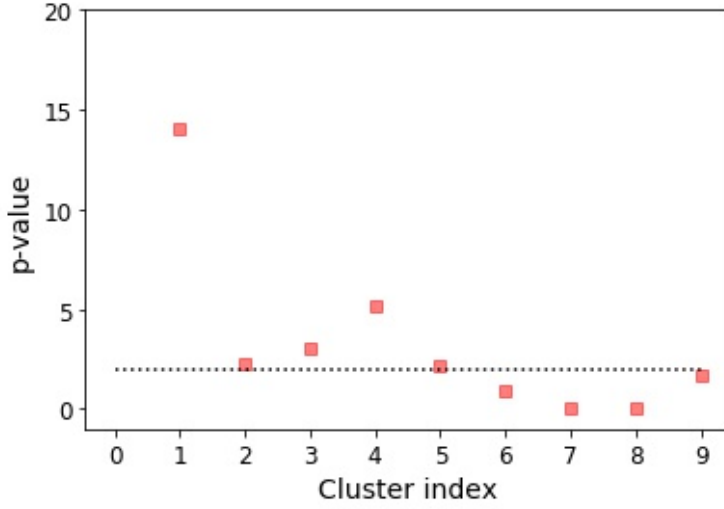


Figure 8: Estimated  $p$  for every cluster. The dash line indicates a value of 2.

## 4.2 Hazard analysis and parametric study

To study the effect of shut-in timing on the short-term hazard, we quantified the short-term hazard as the expected number of times experiencing  $MMI \geq 3$  at the injection site over the next  $T_E$  days given the current injection duration of  $T_S$  days. Figure 1 visualizes the scenario. We focused on the difference between the hazard levels with and without post-shut-in seismicity (i.e., the area highlighted in red in Figure 1).

For simplicity and transparency of results, we assumed a constant seismicity rate during injection, and the Omori model to describe decay of seismicity after the shut-in:

$$\lambda(t) = \begin{cases} \lambda_0 & t \leq T_{SI} \\ \lambda_0 \left(\frac{T_{SI}}{t}\right)^p & t > T_{SI} \end{cases} \quad (6)$$

where  $T_{SI}$  is the actual shut-in time,  $\lambda_0$  is the constant rate before the shut-in, and  $p$  is the parameter describing the post-shut-in decay in seismicity. The actual clusters show time-varying seismicity during injection, as would be expected if hydraulic stimulation is periodically interacting with pre-existing faults and triggering larger earthquakes. However, the constant rate simplifies the model and presentation of results, and if the assumed rate matches the average seismicity rate over the injection period of interest, the numerical results are a reasonable approximation of the more complex case.

The hazard, defined as the expected number of times  $MMI \geq x$  occurs at the injection site over the next  $T_E$  days, can then be computed using:

$$\mu(MMI \geq x, T_E, T_S) = \int_{T_S}^{T_S+T_E} \int_{M_{min}}^{M_{max}} P(MMI \geq x|m) \lambda(t) f_M(m) dm dt \quad (7)$$

where  $P(MMI \geq x|m)$  is the probability of exceeding an MMI given a magnitude  $m$  earthquake, calculated from the intensity prediction equation by Atkinson et al. (2014). We assumed a constant epicenter distance of 2 km and a hypocentral distance of 4 km, estimated based on the information from Yoon et al. (2017).  $\lambda(t)$  is the seismic rate from Equation 6.  $f_M(m)$  is the probability density function for magnitude, assumed here to be a Gutenberg-Richter distribution truncated between magnitudes of 0.2 and 5.0, with  $b = 1.0$  estimated from the nine clusters using the method by Utsu (1965). The lower-bound magnitude corresponds to the magnitude of completeness (though  $M < 1$  events contribute negligibly due to their small resulting ground motion amplitudes). The upper-bound magnitude is much larger than the largest observed event ( $M_L = 2.9$ ), to account for the potential large magnitude due to hydraulic fracturing (e.g., the maximum magnitude of 4.4 in Alberta, Rubinstein and Mahani 2015). Moreover, we observed that adjusting it from 4.0 to 6.0 only results in 5% change in the hazard level in the following results. A site-specific hazard analysis would need to examine the magnitude distribution parameters more closely.

We first conducted a parametric study to see how the hazard varies in this case for a range of values. We considered injection durations ( $T_S$ ) of 2 and 15 days, a time range of interest ( $T_E$ ) of 7 and 30 days, and  $p$  value of 0.7, 2.0, and 4.0. For comparison, we also estimated the hazard if all seismicity stopped after shut-in. We consider an initial post-injection seismicity rate of  $\lambda_0 = 5$  per day, which is the median rate at the time of shut-in for the nine clusters.

Figure 9 summarizes the hazard levels for the considered cases. The x-axis shows the amount of additional time for which injection is continued, with continued injection assumed to produce earthquakes with a mean rate of  $\lambda_0 = 5$  per day, and stopped injection resulting in Omori-decaying seismicity. That is  $x = 0$  on the plot corresponds to immediate shut-in, and  $x = 7$  corresponds to shut-in one week in the future. The y-axis shows the expected number of felt (i.e.  $MMI > 3$ ) events in the next  $T_E$  days. Each solid and dashed line in the figure corresponds to one combination of parameter values, and the black dotted line shows results without post-shut-in seismicity.

All cases with post-shut-in seismicity exceed the case with no post-shut-in seismicity, but the difference between the two depends on the values of parameters. The longer the injection is continued, the higher the hazard, because of the longer interval with higher seismicity. The maximum hazard occurs when the injection duration exceeds the time range of interest (i.e.,  $T_{SI} \geq T_S + T_E$ ) as shown in Figure 9a. The lower the  $p$  (i.e., the slower the decay of post-shut-in seismicity), the higher the hazard. Finally, the larger the  $T_S$  (i.e., the longer the current injection time), the

higher the hazard level. This suggests that the effect of post-shut-in hazard is more significant for long-time injection.

Figure 9 shows that the post-shut-in seismicity could be important for decision-making. For example, for a  $T_S = 15$ -day injection interval, a typical value of  $p = 2$ , and a planned shutdown in 6 days, the 30-day hazard level is forecast to be more than double when considering post-shut-in seismicity than when neglecting it. Post-shut-in seismicity clearly plays a large role in short-term hazard analysis, especially for cases with low  $p$  values and longer injection durations.

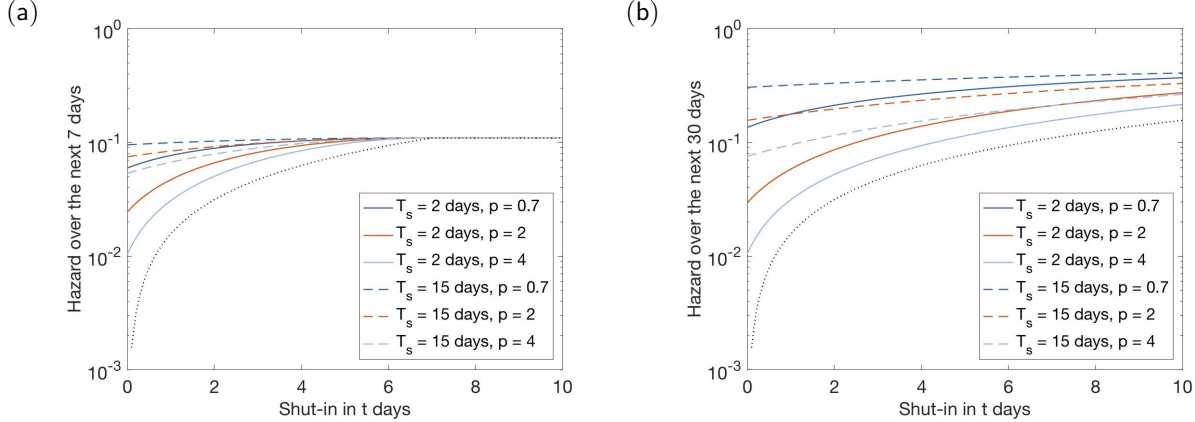


Figure 9: Hazard over the next (a) 7 days and (b) 30 days for different shut-in times. The hazard is defined as the expected number of times experiencing  $MMI \geq 3$  at the injection site. The dotted line corresponds to the case without post-shut-in seismicity.

### 4.3 Sensitivity analysis

We conducted a sensitivity analysis on the  $p$  in the Omori model and  $b$  in the Gutenberg-Richter distribution to consider the uncertainty in the parameter estimation. In particular, both parameters could be estimated using maximum likelihood estimation based on the observed cluster, and we use bootstrapping to quantify the parameters’ uncertainty. We randomly sampled post-shut-in earthquakes with replacement for every cluster and estimated the  $p$  and  $b$  using maximum likelihood estimation. We repeated the process 2,000 times and plotted the distribution of estimated  $p$  and  $b$ . Figure 10 summarizes the estimated values for every cluster. Clusters 1 and 3 have larger numbers of post-shut-in earthquakes than Clusters 2 and 4, but Clusters 2 and 3 have the least  $p$ -value uncertainty due to their more stable decay of seismicity. Moreover, for clusters that are not as well described by a single decay model (i.e., Clusters 5 to 9), their  $p$  values are nearly constant and many are close to 0. The low parameter variability in those cases is due to model mismatch with data rather than true lack of parameter uncertainty, so this sensitivity analysis alone is not sufficient to evaluate model performance. For  $b$  values, the clusters are more comparable in their uncertainty, and the uncertainty decreases relative to the number of post-shut-in earthquakes.

We conducted the sensitivity analysis focusing on clusters that follow a single decay process (i.e., Clusters 1 to 4). However, the results of all clusters are provided in the appendix. In particular, we compared the post-shut-in hazard levels using three sets of  $p$  and  $b$  values: 1) the median values for both  $p$  and  $b$  as a reference hazard level, 2) decreasing one parameter to its 25<sup>th</sup> percentile, 3) decreasing the other parameter to its 25<sup>th</sup> percentile. The parameters are varied asymmetrically in this way in order to understand the potential for adverse outcomes: a lower  $b$  indicates a higher probability of a large-magnitude earthquake, and a lower  $p$  indicates higher post-shut-in seismicity.

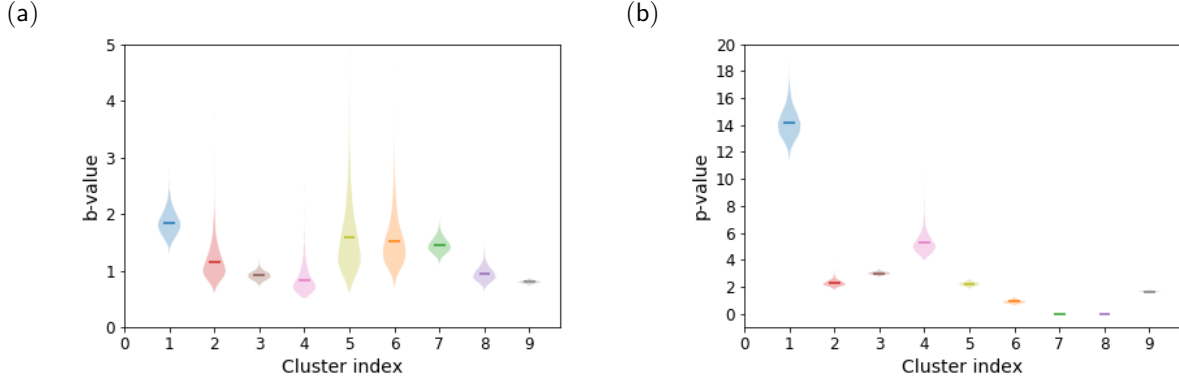


Figure 10: The distribution of the estimated (a)  $b$  and (b)  $p$  for every cluster using bootstrapping. The shaded area corresponds to rotated kernel density plots on both sides. The horizontal line is the mean value.

The  $p$  and  $b$  values could take higher values as well, but those outcomes are of less concern because they are less likely to produce felt shaking.

We computed the hazard levels in the next 7 days for various MMI thresholds using Equations 6 and 7, an injection duration of  $T_S = 2$  or 15 days, and  $T_{SI} = T_S$  (i.e., shutting down immediately). Figure 11 reports the hazard associated with exceeding a range of MMI levels, plotted as the ratio of hazard for a given case relative to the reference case. The reference case uses the median values of  $p$  and  $b$  from Figure 10. The considered comparison cases are the one with a 25<sup>th</sup> percentile  $p$  value or a 25<sup>th</sup> percentile  $b$  value (with  $b$  estimated either from the entire cluster, or from only the post-shut-in events). The solid lines correspond to  $T_S = 2$  days and the dashed lines correspond to  $T_S = 15$  days. In Figure 11, the effect of  $p$  is constant over various MMI thresholds, because the change in  $p$  only affects the seismic rate (i.e.,  $\lambda(m_{min} \leq M \leq m_{max})$ ). However, it varies with the injection duration ( $T_S$ ) - it is more significant with a shorter injection duration. The effect of  $b$  changes with MMI - the hazard for larger MMIs increases more significantly than smaller MMIs. This is because a smaller  $b$  suggests higher probabilities of large-magnitude earthquakes, which contribute to hazard at large MMIs.

We also estimated  $b$  using the entire cluster and included the results in Figure 11. This often results in a smaller standard error than the  $b$  estimated from post-shut-in earthquakes only, thus a smaller increase in the seismic hazard (Figure 11). Most of the time, the uncertainty in  $b$  has a higher impact on the resulting hazard level than  $p$  if both are estimated from the same number of earthquakes. However, the relative importance of  $b$  and  $p$  also depends on the injection duration and MMI thresholds of interest. The resulting hazard level could be more sensitive to  $p$  for small MMI thresholds (e.g.,  $MMI < 3$ ) and short injection duration (e.g.,  $T_S < 3$  days). On the other hand, the effect of  $b$  dominates the hazard at larger MMIs (e.g.,  $MMI > 3$ ).

## 5 Hazard analysis with logic trees and Bayesian updating

Though the Omori model is simple for parameter estimation and model interpretation, it fails to describe cases when there are delayed earthquake clusters after shut-in or when the seismicity increases after shut-in (e.g., Clusters 7 and 8). The earthquake rate is capped at  $\lambda_0$  for the Omori model, and this could result in an underestimation of the post-shut-in hazard. On the other hand, the stretched exponential model could describe the delayed earthquake cluster, thus capture the increase in the post-shut-in hazard. We developed a logic tree by assembling the two models to take

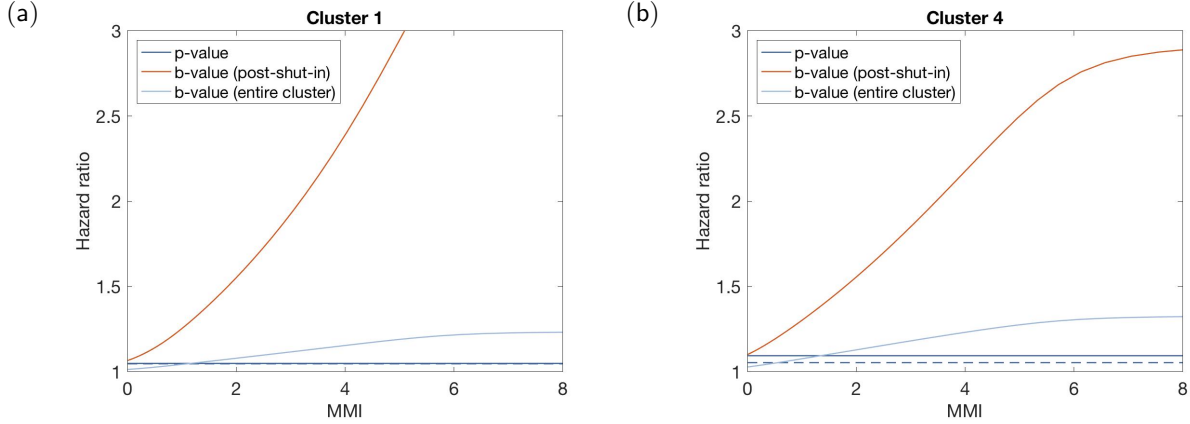


Figure 11: Sensitivity analysis for (a) Cluster 1 and (b) Cluster 4. Hazard results for a 25<sup>th</sup> percentile parameter value are shown, relative to hazard results with median parameter values from Figure 10. The solid lines correspond to  $T_S = 2$  days and the dashed lines correspond to  $T_S = 15$  days.

into account the possibility of increasing post-shut-in seismicity. The logic tree has been used in probabilistic seismic hazard analysis to capture the epistemic uncertainty (Kulkarni et al., 1984). Each branch of the logic tree is a set of possible models with an assigned weight, and the final output is their weighted average:

$$\mu_{average} = \sum_i^N w_i \mu_i \quad (8)$$

where  $w_i$  is the weight for each branch,  $\mu_i$  is the corresponding outcome, and  $N$  is the total number of branches. We developed a logic tree to quantify the post-shut-in hazard. Figure 12 shows a sample logic tree model, with some assumed parameter values and branches. It consists of the stretched exponential model and the Omori model. For each model, the logic tree also considers the uncertainty in the parameters (i.e.,  $p$ ,  $\tau$ , and  $\beta$ ). In Figure 12,  $w_1$  and  $w_2$  represent the weight for the two models, and  $w_{ij}$  is the weight for the corresponding parameters. For illustration, we set all weights according to the nine clusters. According to BIC values of the nine clusters, five of them could be better described by the stretched exponential model, thus we assumed  $w_1 = 0.45$  and  $w_2 = 0.55$ . Assuming  $p$ ,  $\beta$  and  $\tau$  are positive, we defined that  $p$  follows a lognormal distribution and  $\log(\tau)$  and  $\log(\beta)$  follow a multivariate Gaussian distribution. Their parameters were estimated based on the nine clusters. In particular, we excluded Clusters 7 and 8 when constructing the distribution for  $p$ , because the estimated  $p$  for the clusters is zero. In order to quantify the uncertainty, we implemented the Monte Carlo simulation to generate 2,000 sets of parameters according to predefined distributions, and computed the hazard using  $w_1 = 0.45$  and  $w_2 = 0.55$ . The hazard was defined as the expected number of times experiencing  $MMI \geq 3$  in the next 7 days, given a two-day injection. In particular, we set  $\lambda_0 = 5$  per day,  $T_S = 2$  days and  $T_E = 7$  days. Figure 13 shows short-term hazard levels computed using Equations 6 and 7. The solid line is the median hazard level, and the dashed lines correspond to the 10<sup>th</sup> and 90<sup>th</sup> percentiles. We also included the cases for  $w_1 = 1.0$  (i.e., the Omori model) and  $w_1 = 0$  (i.e., the stretched exponential model) for reference. Figure 13 shows that the Omori model has lower median hazard levels than the other two. This is expected because the seismic rate is capped at  $\lambda_0$  for the Omori model, but it could be much higher for the stretched exponential model. As a result, the post-shut-in hazard

from the stretched exponential model could exceed the hazard during the injection (i.e., hazard due to the constant seismic rate  $\lambda_0$ ). As shown in Figure 13, the 90<sup>th</sup> percentiles of the stretched exponential model at  $t < 7$  days is higher than the Omori model and the hazard at  $t > 7$  days. The hazard level with  $w_1 = 0.45$  and  $w_2 = 0.55$  is between the other two cases. It also reflects the possibility of increasing post-shut-in seismicity. Thus, the logic tree model could be used to consider the uncertainty in the model selection and parameter estimation.

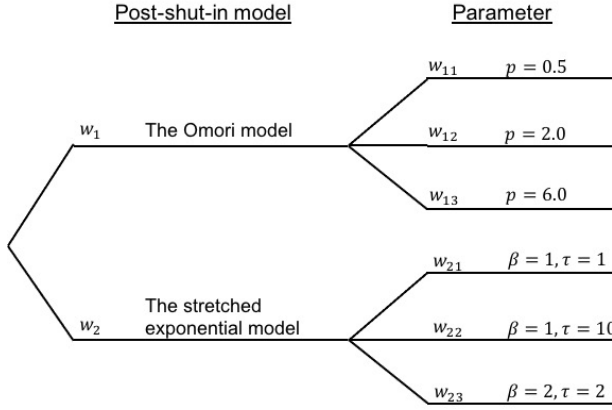


Figure 12: The sample logic tree model, with some assumed parameter values and branches.  $w$  corresponds to the weight for each branch.

All the weights were previously estimated based on the nine clusters, but they could be updated when new injection and earthquake data are available. In particular, we used the Bayes rule to update the weights:

$$w_i^{new} = \frac{L_i w_i}{\sum_i^N L_i w_i} \quad (9)$$

where  $w_i$  is the current weight for a branch and  $w_i^{new}$  is the updated weight.  $L_i$  is the likelihood of observing the new data given the parameters of the branch. The higher the likelihood, the larger the assigned weight.

If we assume that post-shut-in seismicity of nearby wells has similar patterns (e.g., a single decay model), we could update the weights when new injections and clusters are available nearby so that the post-shut-in hazard in the region could be better predicted using the updated weights. For illustration, we assumed that the next five clusters associated with some new injections near Cluster 1 are all similar to Cluster 1 and updated the weights after every cluster. In particular, we generated a new cluster by randomly sampling earthquakes in Cluster 1 with replacement. Figure 14 shows the update in weights for the two models (i.e.,  $w_1$  and  $w_2$ ). They begin with the assumed values (i.e.,  $w_1 = 0.45$  and  $w_2 = 0.55$ ), and after the first cluster, the weight for the Omori model is higher than that of the stretched exponential model, suggesting that the former fits better to the new cluster. The weight for the Omori model decreases slightly after the third cluster, meaning that the stretched exponential model outperforms for this cluster.

We could also update the weights within a cluster when new earthquakes are observed so that the short-term hazard could be updated in real-time. Before shut-in, we estimate the post-shut-in hazard using weights based on some prior knowledge (e.g., the nine clusters). After the shut-in, we update the weights along the time when new earthquakes are observed. We illustrated this process using Cluster 3, where we updated the weights every day based on the earthquakes up to that date,

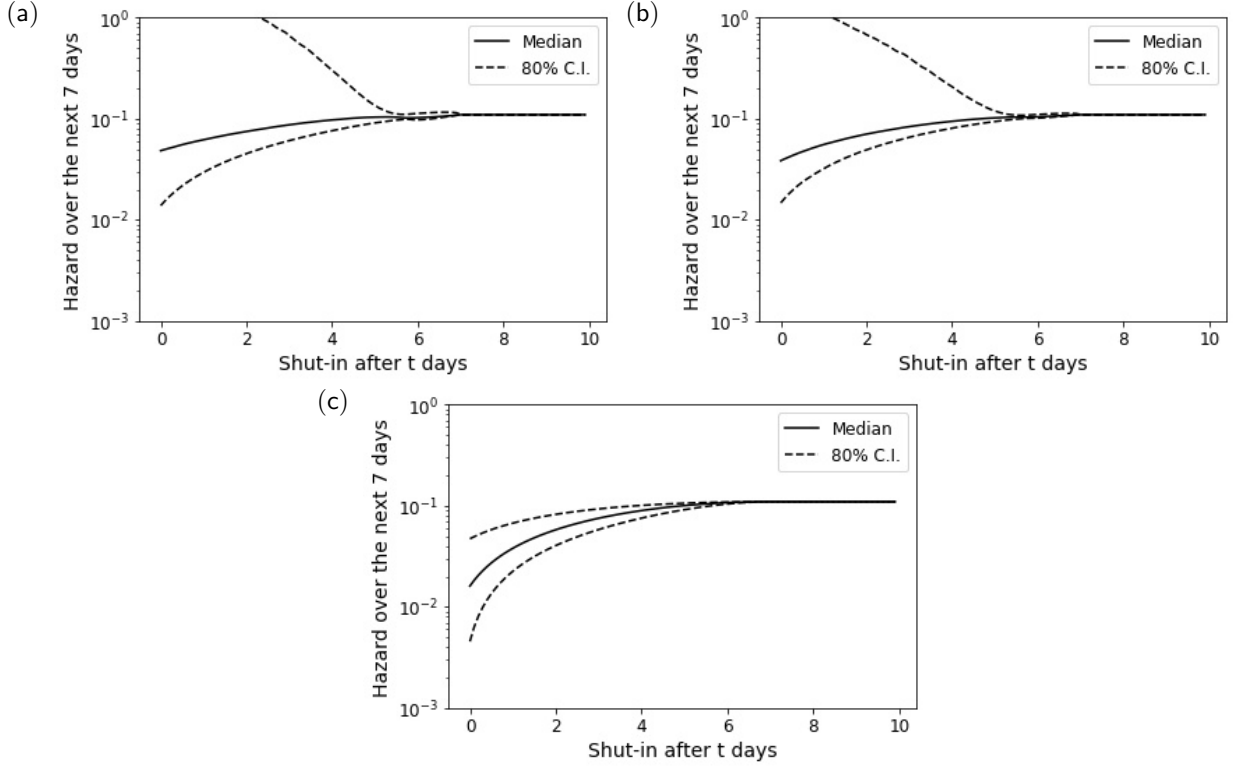


Figure 13: The expected number of times experiencing  $MMI \geq 3$  over the next 7 days for different shut-in times. The weight for the Omori model is (a) 0.0, (b) 0.45, and (c) 1.0. The solid line shows the median values, and dashed lines indicate the 80% confidence interval (C.I.).



Figure 14: Updated weights for the Omori model and the stretched exponential model after five clusters re-sampled from Cluster 1.

and computed the hazard in the next 7 days. The short-term hazard was defined as the expected number of  $MMI > 3.0$  events over the next 7 days. Figure 15a shows the update in weights for the two models (i.e.,  $w_1$  and  $w_2$ ) along the time. The weight for the Omori model increases when

earthquakes are being observed after the shut-in. Figure 15b shows the expected number of times experiencing  $MMI \geq 3$  in the next 7 days based on the updated weights. The hazard decreases along the time because, according to Figures 5 and 15a, the post-shut-in seismicity could be better described as a single decay process (i.e., the Omori model). Moreover, as more earthquakes are collected, the parameters are better constrained, and thus we are more confident on the predicted hazard. Though after the injection, limited actions could be done to control the short-term hazard further, we could better prepare for the coming hazard based on the real-time prediction.

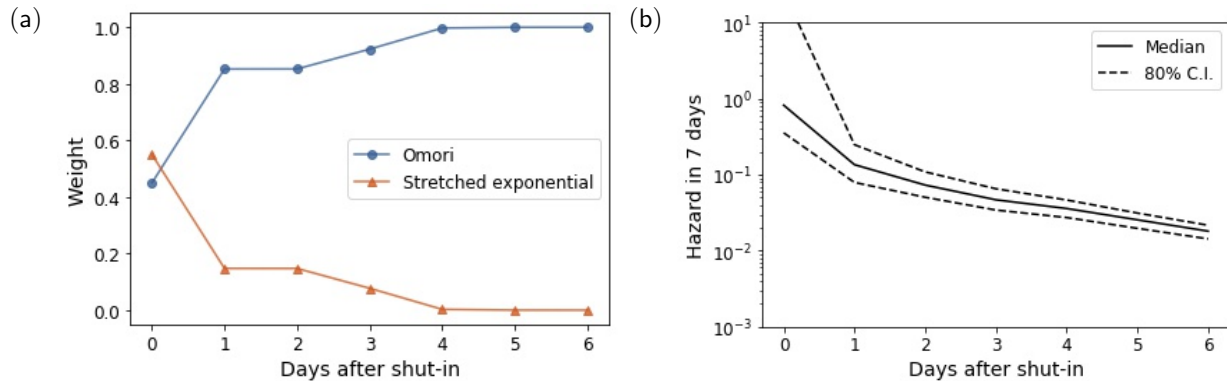


Figure 15: (a) Updated weights for the Omori model and the stretched exponential model after shut-in. (b) The expected number of times experiencing  $MMI \geq 3$  over the next 7 days for different times after the shut-in. The solid line shows the median values, and dashed lines indicate the 80% confidence interval.

The above results consider clusters that are reasonably represented by the Omori model. The same exercise could be repeated for the clusters represented by the stretched exponential model, but the updating exercise is less valuable in those cases. First, because the Omori model works poorly for those clusters, the model weights quickly shift entirely to the stretched exponential model. This is a good verification of the updating algorithm, but less useful for decision-making; when the Omori model is inappropriate, this can be seen visually and the updating procedure is not needed. Second, the forecast hazard can be quite large in these cases, due to the potential for seismicity to continue increasing, and the significant uncertainty on model parameters when activity is increasing. While it is true that the hazard is potentially high in such situations, a manual review of the increasing seismicity may be as informative for decision-making as a quantitative assessment that has significant uncertainty. The updating approach thus has some robustness in providing reasonable results for all clusters, but is most informative in forecasting hazard for situations where seismicity is decaying in time.

## 6 Conclusion

This project evaluated three statistical models to describe the post-shut-in seismicity. We also studied the effect of post-shut-in seismic hazard on decision-making and proposed a logic tree model to incorporate the uncertainty in model selection and parameter estimation.

We considered three statistical models - the Omori model from Langenbruch and Shapiro (2010), the exponential model, and the stretched exponential model from Mignan et al. (2017). They were evaluated based on nine clusters of hydraulic-fracturing-induced earthquakes near the Guy-Greenbrier fault in Arkansas (Yoon et al., 2017). Results suggested that half of the clusters could be

well described by a single decay process. The Omori model performed best for those clusters, with the lowest BIC values (indicating consistency between the data and model), though the stretched exponential model performed almost as well in many cases. There were also clusters where the seismicity increased after the shut-in and could not be described as a single decay process. In these cases, the stretched exponential model worked best. The Omori model had the advantages of 1) performing best for the single decay process, and 2) being easy to estimate and interpret due to the functional form and the number of parameters involved. However, it failed to describe the situation of the increasing post-shut-in seismicity. The stretched exponential model could handle such cases - it could describe both the single decay process and the delayed earthquake cluster. However, compared to the Omori model, it could result in unrealistic estimated rates: a discontinuous and extreme rate right after shut-in. Given its stability and ease of use, we used the Omori model to study the effect of post-shut-in hazards on decision-making. We also considered a logic tree model to incorporate the possibility of other post-shut-in patterns.

We defined the short-term hazard as the expected number of times exceeding an MMI of 3.0 at the injection site in the next  $T_E$  days given the current injection duration of  $T_S$  days. We first conducted a parametric study on the seismicity decay parameter  $p$  and the injection duration  $T_S$ . Higher  $p$  implies more rapid decay in the seismicity and thus lower post-shut-in hazard. Keeping other parameters unchanged, the longer the current injection time ( $T_S$ ), the higher the hazard level. This suggests that the post-shut-in hazard is more important for a long-time injection. Comparing the hazard computed with and without post-shut-in seismicity, we observed that the post-shut-in hazard could be important to decision-making in some cases. For example, assuming  $T_S = 15$  days and  $p = 2$  and a target 30-day hazard of 0.1 (i.e.,  $\mu(\text{MMI} \geq 3) < 0.1$ ), an analysis ignoring post-shut-in seismicity would imply that continued injection for 6 days is acceptable. However, analysis considering post-shut-in seismicity would suggest that injection should shut down immediately. If we continue the injection for 6 days, the hazard could increase by more than 100%.

We also studied the effect of parametric estimation uncertainty (i.e.,  $p$  for the Omori model and  $b$  for the Gutenberg-Richter distribution) on the estimated hazard. Results showed that the uncertainty in  $b$  has a higher impact on the resulting hazard level than  $p$  if both were estimated from the same number of earthquakes. However, the relative importance of  $b$  and  $p$  also depends on the injection duration and MMI thresholds of interest. The hazard is more sensitive to  $p$  for small MMI thresholds (e.g.,  $\text{MMI} < 3$ ) and short injection duration (e.g.,  $T_S < 3$  days). On the other hand, the effect of  $b$  dominates the hazard at larger MMI thresholds (e.g.,  $\text{MMI} > 3$ ).

We proposed a logic tree model to incorporate the uncertainty in model selection and parameter estimation. As an example, we developed a logic tree that considered the possibility of seismicity following either the Omori model or the stretched exponential model. This model captured the possibility of increasing post-shut-in seismicity and hazard. The weights of each branch could be updated in a Bayesian manner as new post-shut-in data is observed. We illustrated the process of tree construction and weight updates using the nine earthquake clusters in Guy-Greenbrier, Arkansas (Yoon et al., 2017).

## 7 Acknowledgements

This research was sponsored by the Stanford Center for Induced and Triggered Seismicity. We thank Pierre-Francois Roux and an anonymous reviewer for feedback that significantly improved the final manuscript. Both earthquake and injection data were collected from Yoon et al. (2017). The data generated during and/or analysed during the current study are available from the corresponding author on reasonable request.

## References

- Atkinson GM, Worden CB, Wald DJ (2014) Intensity prediction equations for north america. *Bulletin of the Seismological Society of America* 104(6):3084–3093
- Bachmann CE, Wiemer S, Woessner J, Hainzl S (2011) Statistical analysis of the induced basel 2006 earthquake sequence: introducing a probability-based monitoring approach for enhanced geothermal systems. *Geophysical Journal International* 186(2):793–807
- Barth A, Wenzel F, Langenbruch C (2013) Probability of earthquake occurrence and magnitude estimation in the post shut-in phase of geothermal projects. *Journal of seismology* 17(1):5–11
- Broccardo M, Mignan A, Wiemer S, Stojadinovic B, Giardini D (2017) Hierarchical bayesian modeling of fluid-induced seismicity. *Geophysical Research Letters* 44(22):11–357
- Chang KW, Yoon H, Martinez MJ (2018) Seismicity rate surge on faults after shut-in: Poroelastic response to fluid injection. *Bulletin of the Seismological Society of America* 108(4):1889–1904
- Deichmann N, Giardini D (2009) Earthquakes induced by the stimulation of an enhanced geothermal system below basel (switzerland). *Seismological Research Letters* 80(5):784–798
- Dieterich JH, Richards-Dinger KB, Kroll KA (2015) Modeling injection-induced seismicity with the physics-based earthquake simulator rsqsim. *Seismological Research Letters* 86(4):1102–1109
- Gischig VS, Wiemer S (2013) A stochastic model for induced seismicity based on non-linear pressure diffusion and irreversible permeability enhancement. *Geophysical Journal International* 194(2):1229–1249
- Hainzl S, Ogata Y (2005) Detecting fluid signals in seismicity data through statistical earthquake modeling. *Journal of Geophysical Research: Solid Earth* 110(B5)
- Häring MO, Schanz U, Ladner F, Dyer BC (2008) Characterisation of the basel 1 enhanced geothermal system. *Geothermics* 37(5):469–495
- Kao H, Visser R, Smith B, Venables S (2018) Performance assessment of the induced seismicity traffic light protocol for northeastern british columbia and western alberta. *The Leading Edge* 37(2):117–126
- Kim WY (2013) Induced seismicity associated with fluid injection into a deep well in youngstown, ohio. *Journal of Geophysical Research: Solid Earth* 118(7):3506–3518
- Kulkarni R, Youngs R, Coppersmith K (1984) Assessment of confidence intervals for results of seismic hazard analysis. In: Proceedings of the eighth world conference on earthquake engineering, vol 1, pp 263–270
- Langenbruch C, Shapiro SA (2010) Decay rate of fluid-induced seismicity after termination of reservoir stimulationspost injection seismicity. *Geophysics* 75(6):MA53–MA62
- Majer EL, Baria R, Stark M, Oates S, Bommer J, Smith B, Asanuma H (2007) Induced seismicity associated with enhanced geothermal systems. *Geothermics* 36(3):185–222
- Mena B, Wiemer S, Bachmann C (2013) Building robust models to forecast the induced seismicity related to geothermal reservoir enhancement. *Bulletin of the Seismological Society of America* 103(1):383–393

Teng, G., and Baker, J. W. (2022). "Post shut-in hazard for hydraulic-fracturing-induced earthquakes: Analysis using data from the Guy-Greenbrier earthquake sequence." *Journal of Seismology*. <https://doi.org/10.1007/s10950-021-10068-3>

---

- Mignan A, Broccardo M, Wiemer S, Giardini D (2017) Induced seismicity closed-form traffic light system for actuarial decision-making during deep fluid injections. *Scientific reports* 7(1):1–10
- Reasenberg PA, Jones LM (1989) Earthquake hazard after a mainshock in California. *Science* 243(4895):1173–1176
- Rubinstein JL, Mahani AB (2015) Myths and facts on wastewater injection, hydraulic fracturing, enhanced oil recovery, and induced seismicity. *Seismological Research Letters* 86(4):1060–1067
- Schultz R, Mei S, Pană D, Stern V, Gu YJ, Kim A, Eaton D (2015) The Cardston earthquake swarm and hydraulic fracturing of the Exshaw formation (Alberta Bakken play). *Bulletin of the Seismological Society of America* 105(6):2871–2884
- Schwarz G (1978) Estimating the dimension of a model. *The Annals of Statistics* pp 461–464
- Segall P, Lu S (2015) Injection-induced seismicity: Poroelastic and earthquake nucleation effects. *Journal of Geophysical Research: Solid Earth* 120(7):5082–5103
- Shapiro SA, Dinske C, Langenbruch C, Wenzel F (2010) Seismogenic index and magnitude probability of earthquakes induced during reservoir fluid stimulations. *The Leading Edge* 29(3):304–309
- Utsu T (1965) A method for determining the value of "b" in a formula  $\log n = a - bm$  showing the magnitude-frequency relation for earthquakes. *Geophys Bull Hokkaido Univ* 13:99–103
- Utsu T, Ogata Y, et al. (1995) The centenary of the Omori formula for a decay law of aftershock activity. *Journal of Physics of the Earth* 43(1):1–33
- Wiemer S, Wyss M (2000) Minimum magnitude of completeness in earthquake catalogs: Examples from Alaska, the western United States, and Japan. *Bulletin of the Seismological Society of America* 90(4):859–869
- Yoon CE, Huang Y, Ellsworth WL, Beroza GC (2017) Seismicity during the initial stages of the Guy-Greenbrier, Arkansas, earthquake sequence. *Journal of Geophysical Research: Solid Earth* 122(11):9253–9274

## 8 Appendix

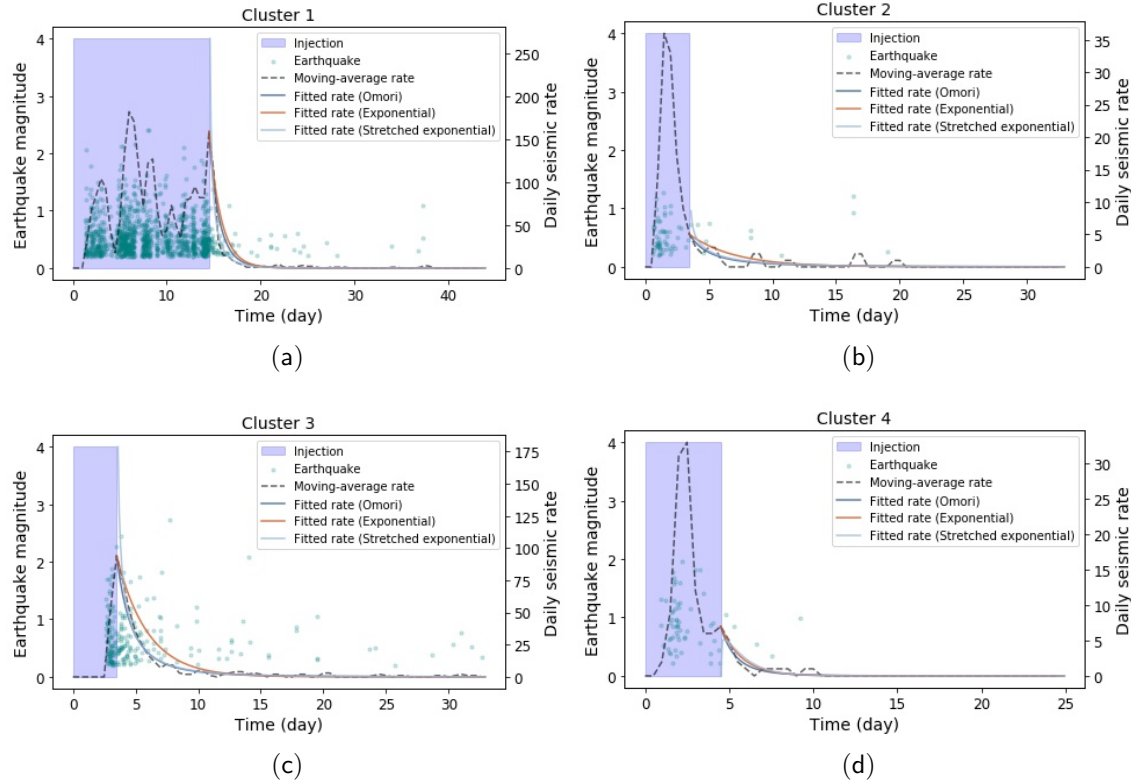


Figure 16: Earthquake occurrence of the nine clusters. The dots are earthquakes, with heights indicating their magnitudes. The shaded area corresponds to the injection. The dashed line is the recorded seismic rate, and the solid lines are the seismic rates using the three fitted models.

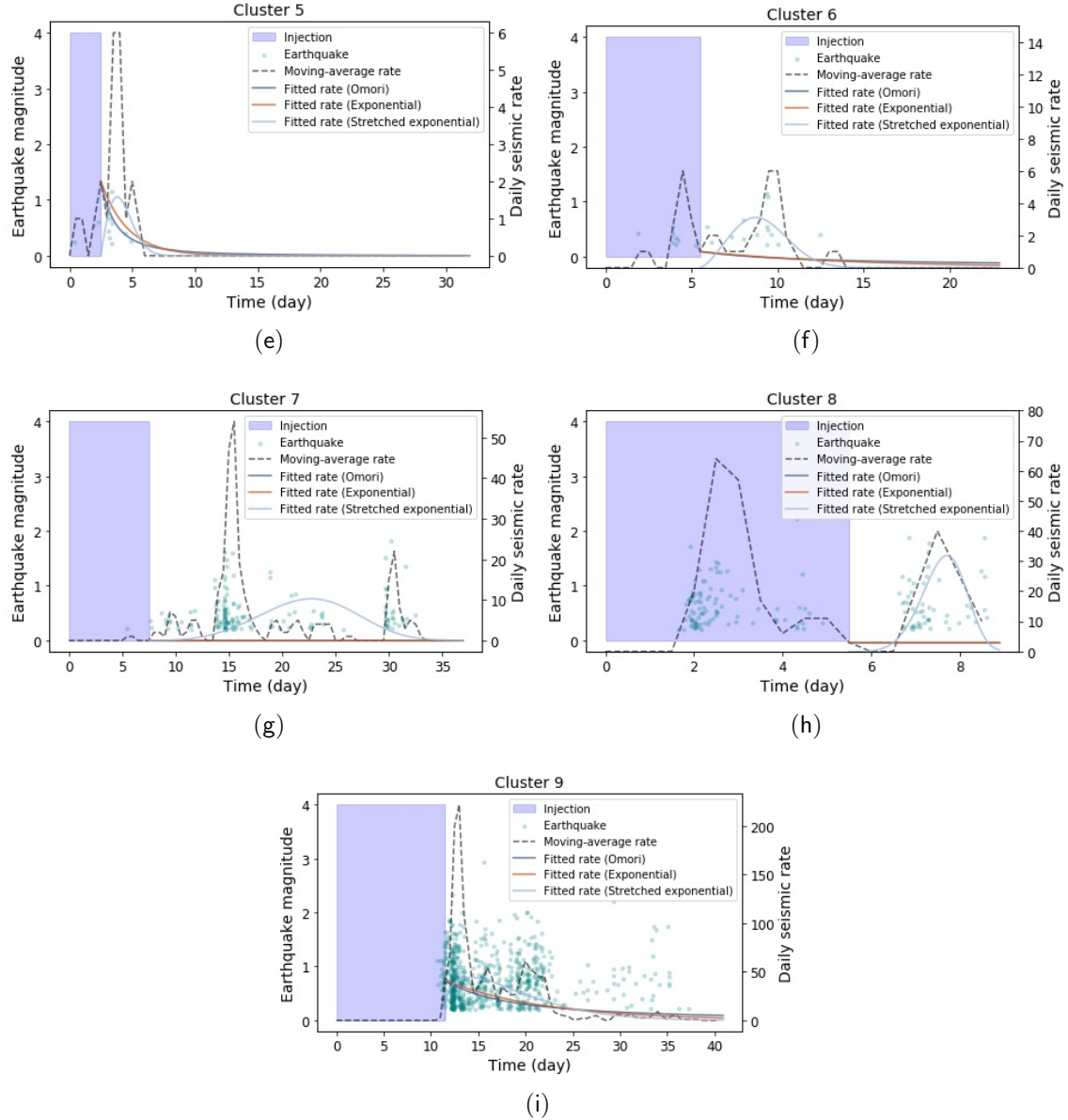


Figure 16: Earthquake occurrence of the nine clusters. The dots are earthquakes, with heights indicating their magnitudes. The shaded area corresponds to the injection. The dashed line is the recorded seismic rate, and the solid lines are the seismic rates using the three fitted models. (cont.)

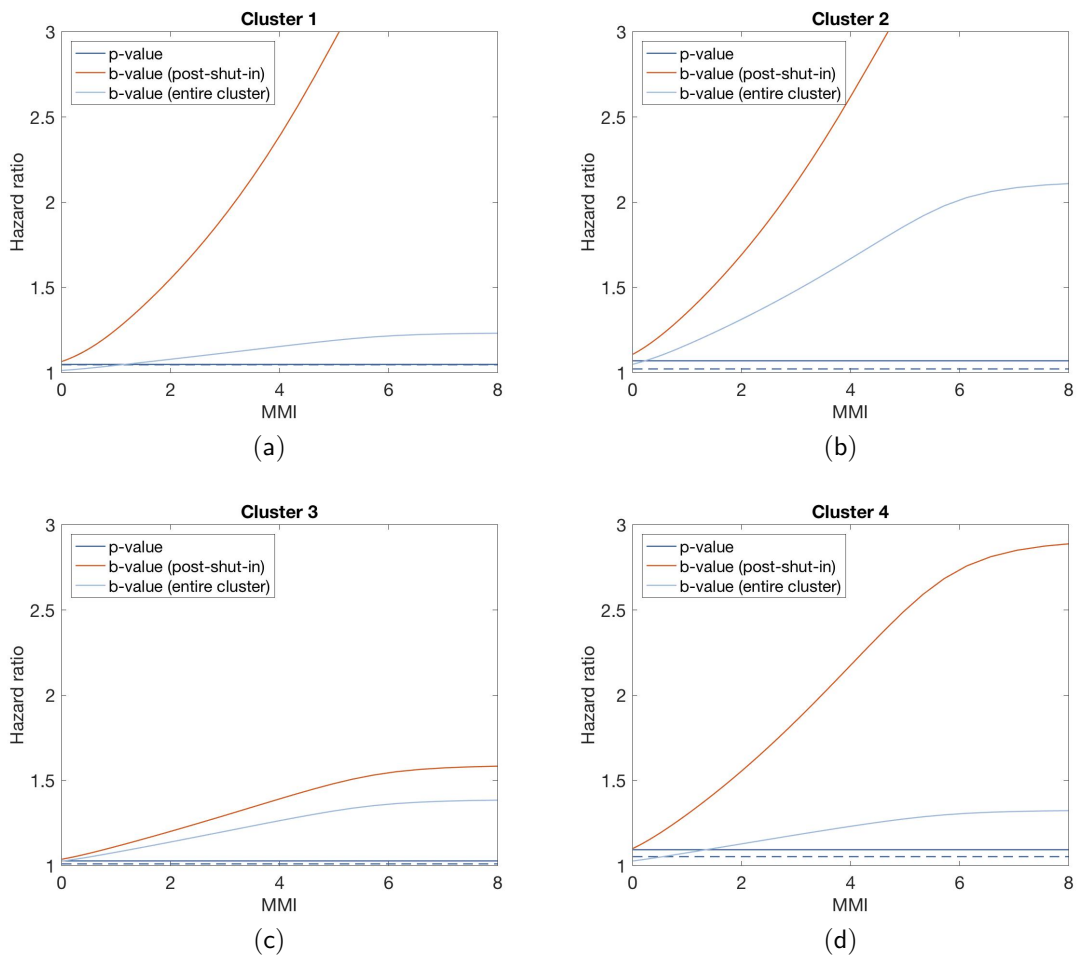


Figure 17: Sensitivity analysis for the nine clusters. The solid lines correspond to  $T_S = 2$  days and the dashed lines correspond to  $T_S = 15$  days.

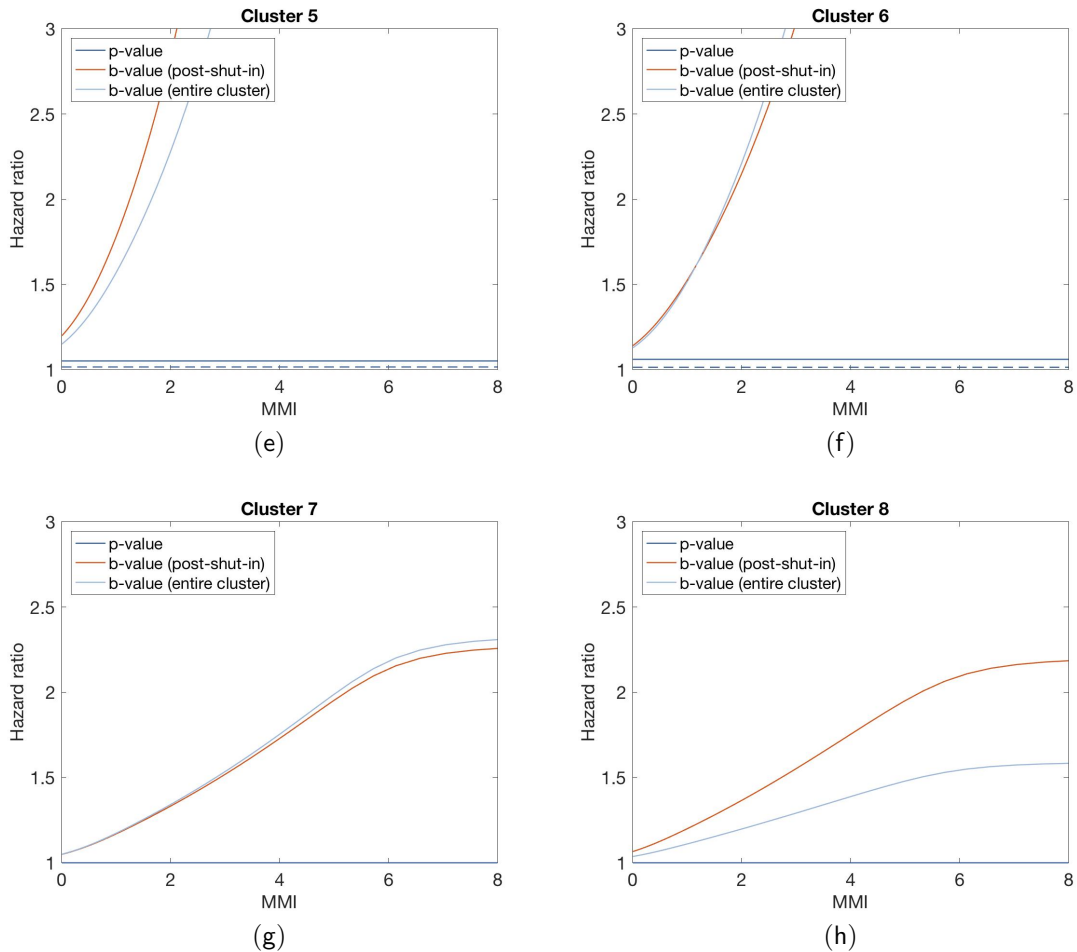


Figure 17: Sensitivity analysis for the nine clusters. The solid lines correspond to  $T_S = 2$  days and the dashed lines correspond to  $T_S = 15$  days. (cont.)

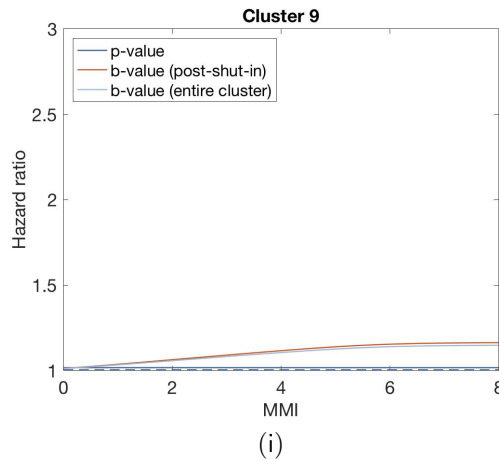


Figure 17: Sensitivity analysis for the nine clusters. The solid lines correspond to  $T_S = 2$  days and the dashed lines correspond to  $T_S = 15$  days. (cont.)